University Library



A gateway to Melbourne's research publications

Minerva Access is the Institutional Repository of The University of Melbourne

Author/s:
Kezia, K;Lee, J;Hill, AJ;Kentish, SE

Title:
Convective transport of boron through a brackish water reverse osmosis membrane

Date:
2013-10-15

Citation:
Kezia, K., Lee, J., Hill, A. J. & Kentish, S. E. (2013). Convective transport of boron through a brackish water reverse osmosis membrane. Journal of Membrane Science, 445, pp.160-169. https://doi.org/10.1016/j.memsci.2013.05.041.

Persistent Link:
https://hdl.handle.net/11343/324545

Convective Transport of Boron through a Brackish Water Reverse Osmosis Membrane

Kezia Kezia[a], Judy Lee[a], Anita Hill[b] and Sandra Kentish[a*]

[a]Particulate Fluids Processing Centre, Chemical and Biomolecular Engineering, University of Melbourne, Parkville, Victoria 3010 Australia

[b]Process Science and Engineering, CSIRO, Clayton South, Victoria 3169, Australia

*Corresponding Author

sandraek@unimelb.edu.au

Abstract

In this work, cross-flow filtration experiments using a brackish water reverse osmosis polyamide membrane have been performed to gather boron rejection data as function of feed concentration, pressure, pH and salinity. Increasing transmembrane pressure increases the permeation of boron indicating that convective flow is important. This result is in contrast to the normal assumption that solution diffusion dominates in such systems. The extended Nernst-Planck equation with a Donnan-steric partition coefficient is used to analyse the transport mechanisms of both neutral boric acid and negatively charged borate ions through the RO membrane. The contribution of surface charge is experimentally determined by streaming potential measurements and the electrokinetic surface charge density is then calculated as a function of ionic strength and pH. It is found that a 0.380 nm pore radius and an effective membrane porosity of 0.05 shows good agreement with experimental data. Charge screening becomes more dominant with increasing ionic strength and this contribution is readily incorporated into the model. The study extends our understanding of the transport mechanism of boric acid and borate ions which can assist in predicting the performance of polyamide reverse osmosis membranes. It also raises questions as to the true mechanism of transport through such a membrane.

1. Introduction

Reverse osmosis is a versatile method that has been widely adopted in water treatment applications such as desalination. Nonetheless, it is often difficult to attain drinking water standards for neutral solutes such as boron using this technique. Boron is present in seawater with average concentrations of 4-6 mg/L [1-6]. Excessive boron consumption can result in health problems, thus, according to the World Health Organization (WHO), the maximum limit for boron in drinking water is 0.5 mg/L [7]. Extensive research has been conducted into boron removal using polyamide reverse osmosis membranes [1, 2, 5, 6, 8-13].

One widely-known mathematical model that has been employed to analyze the rejection of such neutral solutes is the Spielger-Kedem (Kedem-Katchalsky) model [10, 14-16]. This model describes water flux and solute flux as follows:

Equation 1 $$\boldsymbol{J_v = -A\left(\frac{dP}{dx} - \sigma\frac{d\pi}{dx}\right)}$$

Equation 2 $$\boldsymbol{J_s = -B\frac{dC}{dx} + (1-\sigma)J_w\overline{C} = J_v C_p}$$

The permeate flux (J_v) is dictated by both the pressure (P) and osmotic pressure (π) gradient. The effect of the osmotic pressure difference is corrected by a theoretical reflection coefficient (Staverman reflection coefficient, σ) that represents the correction for non-ideality in a semi-permeable membrane $\left(\sigma \equiv \left(\frac{\Delta P}{\Delta \pi}\right)_{J_v=0}\right)$. For an ideal semi-permeable membrane, which passes water but has 100 % rejection of solutes, $\sigma = 1$; while for a completely non-selective porous membranes $\sigma = 0$ [17]. The solute flux (J_s) combines the contribution of a diffusion term (embedded in the solute permeance, B) as well as the convection of bulk solution.

For salt transport through a reverse osmosis membrane, it is generally assumed that $\sigma \sim 1$, due to the high rejection of ions [2, 13, 18-21]. It is argued that as RO membranes possess free volume elements (or pores) that are comparable or smaller in size to the rejected ions, and as these elements fluctuate in position and volume on the time scale of permeation, the active layer of the membrane should be considered as non-porous [22, 23]. This assumption leads to the derivation of the solution-diffusion model [16, 18, 23] in which the flux of solute is independent of the applied pressure (or water flux) and the second term in Equation 2 can be eliminated. This means that the solute flux is only governed by the diffusion (i.e. solute permeance $= B = \frac{DK^L}{l}$) and is no longer affected by the bulk convection. Wijmans and Baker [23] suggest that the transition from a pore flow model to a solution diffusion model occurs at a free volume element size of 5 to 10 Angstroms.

However, the solution diffusion approach has proved less successful in the modeling of boron rejection at lower pH values, and Equations 1 and 2 can better predict the rejection of boron [10, 15]. In this case, $\sigma < 1$, indicating that solute and water transport are not independent and that some convective flow occurs. However, the approach is empirical and does not explain the transport mechanisms across the membrane. Further, it does not include contributions from Donnan exclusion and ion interactions [16, 24]. Finally, the assumptions of a constant reflection coefficient and water permeability carry inaccuracies since these fitted parameters (σ and B) are greatly affected by experimental variables such as pH, pressure and ionic strength [16, 24].

This study focuses on understanding the transport mechanisms across a reverse osmosis membrane by incorporating contributions of both pore size and surface charge. The surface charge of the membrane is experimentally determined by streaming potential measurements. Since the size and number of the free volume elements within a reverse osmosis membrane are not widely reported, the pore radius and the effective membrane porosity are both optimized to match the experimental data. The effects of pH, pressure and ionic strength toward rejection of boric acid and borate ion are investigated and analyzed using a model developed by Bowen and co-workers [25-27]. This model has been extensively used to represent the transport of charged solutes through nanofiltration membranes [28-33]. yet to our knowledge, it has not been applied previously to dense thin-film reverse osmosis membranes. We show that this model can satisfactorily represent the transport of small molecules, both charged and uncharged, through a reverse osmosis membrane. The approach can provide a more sophisticated understanding than the solution diffusion model which is more commonly used.

2. Theoretical aspects

In seawater, boron commonly exists as the neutral boric acid (H_3BO_3). This is a Lewis acid that undergoes dissociation as well as hydrolysis following Reactions 1 and 2 [8, 9, 12, 34, 35]:

Reaction 1 $H_3BO_3 \leftrightarrow H_2BO_3^- + H^+$

Reaction 2 $H_3BO_3 + H_2O \leftrightarrow B(OH)_4^- + H^+$

However, boric acid is electron deficient and so Reaction 2 is favoured [12, 36]. This electron deficiency also causes boric acid to have a large crystal radius that results in poor hydration [12]. As a consequence, boric acid has a small hydrated radius; reported to be between 0.244 -0.261 nm [12, 35].

The dissociation of boric acid through Reaction 2 is affected by pressure, temperature and ionic strength [12, 37]. At a standard temperature of 20 °C, the apparent pKa varies from 9.23 to 8.60 as the salinity varies from 0 to 400 g/L [5, 12, 36, 38]:

$$\boldsymbol{p_{kA} = [B(OH)_4^-][H^+]}$$

Figure 1 presents the percentage of boric acid ionised with respect to pH and salinity based on this pKa data. For concentrations of boron lower than 22 mg/L, the formation of poly-borate compounds is negligible, therefore only $B(OH)_4^-$ and H_3BO_3 primarily exist in the solution [12, 39].

2.1 Rejection of uncharged solutes

At very dilute concentrations, where activity coefficients can be assumed equal to unity, the flux of an uncharged solute such as boric acid is given by the balance between diffusion and convective flow [25-27, 40]:

Equation 3 $$\frac{j_s}{A_k} = \frac{J_v C_{ip}}{A_k} = \frac{K_{ic} c_i J_v}{A_k} - \boldsymbol{D_{ip}} \frac{dc_i}{dx} - \frac{c_i D_{ip}}{RT} \boldsymbol{V_{is}} \frac{d(P-\pi)}{dx}$$

Where the solute (j_s) and solution (J_v) fluxes are determined on a membrane area basis by accounting for the membrane effective porosity, (A_k). D_{ip} is the diffusion coefficient in the pore, K_{ic} the convective hindrance factor, V_{is} *is* the partial molar volume of the solute. C_{ip} represents the bulk

permeate concentration of the solute *i,* while c_i is the concentration within the pore at any position x. The net pressure gradient across the membrane is given by the difference between the bulk pressure *(P)* and the osmotic pressure *(π)* as a function of the distance through the membrane (x).

This pressure gradient can be related to the volumetric solution flux if it is assumed that the membrane pores are cylinders and that flow through these cylinders can be described using the Hagen-Poiseulle equation:

Equation 4 $$\boldsymbol{J_v = \frac{r_p^2}{8\eta\left(\frac{\Delta x}{A_k}\right)}(\Delta P - \Delta \pi)}$$

Where η is the solvent viscosity, r_p is the pore radius and Δx is the thickness of the active layer of the membrane. This approach assumes that the entire pressure drop occurs across this active layer and there is no significant pressure drop across the support layer. It also assumes that concentration polarisation is insignificant. If the pressure drop is assumed to be linear across the membrane thickness:

Equation 5 $$\boldsymbol{\frac{d(P-\pi)}{dx} = \frac{8J_v\eta}{r_p^2 A_k}}$$

Rearranging the equations above, the concentration gradient across the membrane is calculated

Equation 6 $$\boldsymbol{\frac{dc_i}{dx} = \frac{J_v}{D_{ip}A_k}\left[\left(K_{ic} - \frac{D_{ip}}{RT}V_{is}\frac{8\eta}{r_p^2}\right)c_i - C_{ip}\right]}$$

K_{ic} and K_{id} can be calculated based on the ratio of solute to pore radius (Table 1). D_{ip} is then determined from the bulk diffusion coefficient as $\boldsymbol{D_{ip} = K_{id}D_\infty}$.

For uncharged solutes, the boundary conditions for this equation are given by the steric partition coefficient Φ_i which is a function only of the ratio of the solute and pore radii ($\Phi_i = (1-\lambda)^2$):

Equation 7 $$\boldsymbol{\frac{c_{i\,x=0}}{C_{if}} = \frac{c_{i\,x=\Delta x}}{C_{ip}} = \Phi_i}$$

Integrating Equation 6, the rejection of uncharged solute can then be estimated as follow:

Equation 8 $$\boldsymbol{R = 1 - \frac{C_{ip}}{C_{if}} = 1 - \frac{\left(K_{ic} - \frac{D_{ip}}{RT}V_{is}\frac{8\eta}{r_p^2}\right)\phi}{1-\exp(-P_e')\left[1-\phi\left(K_{ic} - \frac{D_{ip}}{RT}V_{is}\frac{8\eta}{r_p^2}\right)\right]}}$$

Where P_e' is a modified Peclet number given by $\frac{\left(K_{ic} - \frac{D_{ip}}{RT}V_{is}\frac{8\eta}{r_p^2}\right)J_v\,\Delta x}{D_{ip}A_k}$. The properties of the membrane such as the ratio of thickness to porosity ($\frac{\Delta x}{A_k}$) as well as the pore radius are commonly determined through fitting water flux and neutral solute rejection data to Equations 4 and 8. The effective membrane porosity A_k can then be estimated provided that the membrane thickness is known.

2.2.2. Rejection of ions

The transport of ions is further complicated by the addition of an electrochemical potential. Utilisation of the Extended Nernst-Planck equation leads to:

Equation 9 $$\frac{dc_i}{dx} = \frac{J_v}{A_k D_{ip}}\left[\left(K_{ic} - \frac{D_{ip}}{RT}V_{is}\frac{8\eta}{r_p^2}\right)c_i - C_{ip}\right] - \frac{z_i c_i F}{RT}\frac{d\psi}{dx}$$

Equation 10 $$\frac{d\psi}{dx} = \frac{\sum\frac{z_i J_v}{A_k D_{ip}}\left[\left(K_{ic} - \frac{D_{ip}}{RT}V_{is}\frac{8\eta}{r_p^2}\right) - C_{ip}\right]}{\frac{F}{RT}\sum z_i^2 c_i}$$

The electroneutrality condition also leads to the constraint that:

Equation 11 $$\sum z_i C_i = 0$$

Equation 12 $$\sum z_i c_i = -X_d$$

where X_d is the membrane fixed charge density. Our recent work has indicated that the charge on both sides of the active layer of a polyamide membrane is comparable [41]. Therefore, it is assumed that this charge density is constant.

The electrokinetic surface charge density of the membrane can be calculated from zeta potential data by using the equation reported by Ariza et al [42]:

Equation 13 $$\sigma_s = \frac{2RT\varepsilon_o\varepsilon_r k}{zF}\sinh\left(\frac{F\zeta}{2RT}\right)$$

The contribution of ionic strength is represented as k (1/debye length), where the debye length k^{-1} can be calculated as follows:

Equation 14 $$k^{-1} = \sqrt{\frac{\varepsilon_r\varepsilon_o k_b T}{2N_A e^2 I}}$$

Equation 13 is derived from the Grahame equation [43] and is valid only for zeta potentials measured using symmetrical background electrolytes. The membrane fixed charge density (mol/m^3) can then be estimated by assuming that the surface charge in a pore is equal to the charge on the surface[29, 31].

Equation 15 $$X_d = \frac{2\sigma_s}{F r_p}$$

Boundary conditions at the membrane surface are also no longer just a result of steric effects. Zhu et al. 2011 [31] claims that solvation of ions into the membrane is now governed by both steric exclusion (represented by Φ_i) and the Donnan potential difference between the bulk solution and the membrane structure ($\Delta\psi_D$).

Equation 16 $$\frac{c_{ix=0}}{C_{if}} = \Phi_i \exp\left(-\frac{z_i F}{RT}\Delta\psi_D|_{x=0}\right) \quad ;$$

$$\frac{c_{ix=\Delta\ell}}{C_{ip}} = \Phi_i \exp\left(-\frac{z_i F}{RT}\Delta\psi_D|_{x=\Delta x}\right)$$

The Donnan potential difference ($\Delta\psi_D$) can be determined mathematically at both the membrane interfaces $x = 0\ and\ x = \Delta x$ by substituting Equation 16 into Equation 12, if the charge density is known:

Equation 17

$$\sum z_i \; C_{if} \left[\Phi_i \, exp\left(-\frac{z_i F}{RT} \, \Delta\psi_D|_{x=0}\right)\right]_{x=0} = \sum z_i \; C_{iP} \left[\Phi_i \, exp\left(-\frac{z_i F}{RT} \, \Delta\psi_D|_{x=\Delta l}\right)\right]_{x=\Delta x} = -X_d$$

3. Materials and Methods

3.1 Materials

All chemical reagents utilized were analytical grade. Sodium chloride (NaCl, min 99.0%), sodium hydroxide (NaOH, min 97.0%), hydrochloric acid (HCl, 37.0%), N-N dimethyl formamide (N-N DMF, 98%) and sodium bicarbonate ($NaHCO_3$, 99.7%), were purchased from ChemSupply, boric acid (H_3BO_3, 99.5%) was purchased from Merck and sodium tungstate dihydrate ($Na_2WO_4.2H_2O$, 99.0%) was purchased from Sigma Aldrich. The reagents were used as received without further purification. Water utilized for filtration experiments had a resistivity greater than 15.5 MΩ-cm, while buffer and stock solutions for analysis were prepared using water with resistivity greater than 18.2 MΩ-cm.

The membrane utilized in this study was a brackish water membrane, BW30LE provided by Dow Filmtec© and supplied as dry coupons. This membrane is believed to be an uncoated polyamide material on a polysulfone support Prior to any experiment, the membrane was rinsed and soaked overnight in purified water to ensure maximum hydration.

3.2 Experimental Methods.

Filtration experiments were conducted utilizing a cross flow filtration rig (Figure 2) consisting of three parallel cells (Sterlitech CF042). Each cell had a membrane feed channel of width 4.6 cm, length 9.2 cm and depth 2.3 mm. A low foulant (34 mil) feed side spacer (Sterlitech) was used to minimise concentration polarisation. The feed flow was delivered by a Hydra-Cell G10 positive displacement pump (Warner Engineering). The feed line was immersed in a water bath to maintain a temperature of 25°C and the line pressure was monitored using a digital pressure indicator (C62 series, Hydracell). The retentate was recirculated back to the feed tank through back pressure regulators (Swagelok BP-60 Series) and flow meters (Blue-White Industry). The pressure was monitored using analogue pressure indicators (Floyd) connected independently to each cell.

Prior to conducting any experiment, the hydrated membrane was compressed at 2000 kPa for 8 hours using deionised water. The boron concentration in the feed tank was prepared to a concentration of 0 to 20 mg/L by adding H_3BO_3. The pH was adjusted by the addition of NaOH or HCl 2 M. In studying the effect of ionic strength on boron rejection, NaCl was added to adjust the salinity from 0.5 g/L up to 15 g/L. A pH meter (Orion 720A+) and conductivity meter (CRISON basic 30+) were utilised to monitor pH and salinity, respectively. The water flux was measured by weighing the amount of permeate in 5 minute intervals. All experiments were repeated three times for consistency. Concentration polarization was determined using the Sutzkover [44] method and found to be negligible as the concentrations used were low and spacers were employed.

Inductively coupled plasma optical emission spectroscopy (ICP-OES, 720ES, Varian) was used to analyse the boron concentration in both the feed and permeate. This instrument is sensitive to 0.1 $\mu g/L$ boron. Standard solutions ranging from 0 to 50 mg/L of boron were used for calibration.

An Electro Kinetic Analyser (EKA, Anton Paar GmbH) was utilised to measure the streaming potential of the membrane. Two membranes with the active layers facing each other were mounted in a rectangular cell. A PTFE spacer with thickness 0.28 mm was used to create a flow channel. The potential difference was detected using reversible Ag/AgCl electrodes and the data then utilised to calculate the zeta potential value by employing Helmholtz-Smoluchowski equation with Fairbrother and Matsin substitution. The zeta potential was measured using a background electrolyte of 0.6 $\pm$ 0.05 g/L (9.8 $\pm$ 1.3 mM) NaCl [2, 11] and boron additions of 0 to 20 mg/L. An experiment varying pH from 3 to 10.5 was also conducted by adding 0.1 M NaOH or HCl to increase or decrease the pH respectively.

The thickness of the polyamide layer within the BW30LE membrane was measured using Scanning Electron Microscope (SEM). The polyester support layer was physically peeled off and the flattened polyamide-polysulfone layer was mounted on circular templates of 0.5 cm diameter. Samples were then washed using N-N DMF until the polysulfone layer was completely dissolved and then rinsed with Milli-Q water [41, 45]. The polyamide layer was dried at room temperature and then crushed to acquire sharp edges for cross-sectional thickness measurement.

The membrane thickness was also confirmed using Transmission Electron Microscopy (TEM). The polyester backing layer was peeled off and the polyamide-polysulfone layer was stained using Na_2WO_4 as describe by Freger [46]. The sample was immersed in 1mM HCl and then immersed in 5% Na_2WO_4 solution for 15 mins. The stained membrane was washed using deionised water followed by EtOH and air dried at 50^{o}C. Finally, the sample was fixed in araldite resin and sliced using an ultramicrotome to size 60-90 nm for TEM measurement.

3.3 Mathematical Modelling.

The solute data using in modelling is provided in Table 2. MATLAB® R2012b was utilised as the computational software to fit the relevant equations to the experimental data. A block diagram outlining the sequence of calculation is provided in Figure 3.

4. Results and Discussion

4.1. Preliminary Experiments

The charge within a membrane structure is affected by both pH and ionic strength. Increasing pH causes the surface potential to become more negative until a plateau value is reached at about pH 10 (Figure 4a). This is due to protonation of amine groups at low pH and deprotonation of carboxylate groups at high pH. Beyond pH 12 (OH^- = 10 mM), the concentration of NaOH added to the solution exceeds the background electrolyte concentration, causing the measured potential to decline further. However, it is generally accepted that this further decline is an experimental artefact and hence in later modelling a constant value (at pH ≈ 10.5, where NaOH is 3 % of the background electrolyte concentration) is taken as the zeta potential value at all pH values in excess of 10.5.

Increases in the ionic strength cause the streaming potential value to become less negative at low concentrations (Figure 4b). However, at higher concentrations, the value stabilises as the surface charge is effectively screened by the bulk electrolyte. When the electrolyte concentration is greater than 100mM, the voltage measurement carries a significant error [47]. Hence in our mathematical modelling we assume a constant zeta potential for ionic strengths greater than 100mM. Separate experiments conducted at increasing boron concentrations at this pH (data not shown) confirmed that the addition of borate to a level of 20 mg/L Boron had a negligible effect on this potential.

The streaming potential measurements have been utilised to calculate the electrokinetic surface charge density using Equation 13, with results presented in Figure 5. At higher ionic strengths, the debye length (k^{-1}) is compressed and more charge can accumulate in the vicinity of the membrane. Hence, the magnitude of the charge density increases in an opposite trend to the zeta potential data. The valence, z, in Equation 13 is the valence of the background electrolyte, in this case NaCl, thus a negative streaming potential results in a negative electrokinetic charge density [48, 49].

Accurate measurement of the water flux through the BW30LE is important, as it dictates the transport of the solute via convection. A preliminary run at 2 g/L NaCl was conducted to validate the membrane performance against the manufacturer specifications. A strong linear relationship between water flux and pressure was obtained as expected (Figure 6) with the resulting water permeance (A, Equation 1) consistent with the manufacturer data [50] and independent of the boron concentration. A slight increase in water flux was observed with increasing pH (data not shown). Such an increase has been noted by some groups [21, 51, 52], although Childress and Elimelech [53] indicate that the water flux should reach a maximum at the isoelectric point.

The thickness of the polyamide active layer in BW30LE has not yet been widely reported. A wide variation of thickness was observed across the membrane area when SEM and TEM measurements were conducted. An average value of 105 $\pm$ 36 nm was utilised in the model, based upon these measurements. As above, this membrane thickness and pore size might change due to swelling depending upon the pH of the solution, the degree of hydration as well as the salinity. However,

Freger [45] reports that for heavily cross-linked reverse osmosis membranes, the maximum swelling is approximately 11% of the dry thickness. This degree of swelling is within the error bars of the thickness measurement itself. Hence, to simplify the current study, the membrane thickness and pore size of the membrane are assumed to be constant.

4.2 Experimental Results for the Rejection of Boron

It is known that the rejection of boron is primarily controlled by the rejection of borate ions. As shown in Figure 7, at low pH the rejection is low, reflecting the low concentrations of this ion (Figure 1). Minimum ion rejection is commonly observed at the isoelectric point [24, 53]. However, in this case at the isoelectric point (pH =4, Figure 4), less than 0.1 % of boric acid is ionised and since the rejection of neutral solute is unaffected by the membrane charge, no effect is observed. Increases in the rejection are observed at a pH greater than 8 reflecting increasing concentrations of the borate ion. Furthermore, as shown in Figure 5, the surface potential and charge density is more negative at higher pH which will further enhance rejection of negatively charged species.

Figure 8 presents data for the solute flux (J_s) of boron at both pH 2.0 and pH 8.3 as a function of applied pressure. As discussed above, at pH ≤ 8, the boric acid is essentially uncharged (ionised portion < 3.5%, refer to Figure 1Figure **1**). An increase in the solute flux as a function of applied pressure is observed. This is an important finding, as it implies that convective flow cannot be ignored. If the transmission of boric acid were to occur only through solution diffusion, then the solute flux would be independent of pressure [22]. These results show that boron permeation increases with pressure, because it is carried along (convected) with the increasing flux of water. Other workers have similarly found that simple solution diffusion is insufficient to describe the flow of boron through RO membranes and account for this with the use of Equation 1 and Equation **2** and reflection coefficients that are less than unity. In particular, Arias et al [54] show that the reflection coefficient can range between 0.6 – 0.9 for the solute flux of boron between pH 6-9. The nanofiltration model presented by Bowen and co-workers [26] allows for such effects in a more comprehensive manner and so forms the basis of the modelling in this paper.

Further experimental data is presented in Figure 9 to Figure 12 and discussed in the context of the mathematical model in the following section.

4.3 Mathematical Modelling the Rejection of Boron

The rejection at low pH, where boron exists predominantly as the neutral boric acid, is dictated by the steric hindrance. Hence, Equations 3 and 8 were initially utilised to model the experimental data in this pH region. The optimum pore radius (r_p) as well as $\frac{\Delta x}{A_k}$ are estimated through fitting 50 pairs of rejection and flux data for boric acid permeation at pH 2 - 4 (typical fitting results are shown in Figure 7 and Figure 9). The optimised pore radius of 0.380 nm is consistent with previous work. Bowen and co-workers [26, 31, 55] find values of 0.45 - 0.66 nm for a nanofiltration membrane, which would be expected to have larger pore radii, while the pore radius of a seawater RO membrane, which should have tighter pores than the brackish water membrane used here, has been measured utilising PALS (Positron Annihilation Lifetime Spectroscopy) as 0.278 nm [41]. It can be seen that in the low pH region, the predicted boron rejection is very sensitive toward changes in this parameter (Figure 7) due to changes in steric hindrance (Equation 7).

The value of $\frac{\Delta x}{A_k}$ is also determined from the optimisation procedure. The optimised value of 2 μm is consistent with the value presented by Bowen and Mohammad [25]. Utilising the active layer thickness of 105 nm measured experimentally, the effective porosity of the active layer is evaluated to be 0.05. To confirm the validity of this value, the fractional free volume in the active layer was calculated using the well known Bondi method [56], which is usually applied to gas separation membranes. In this case, the volume occupied by the polymer chains is first evaluated from a group contribution method. This can then be converted to a fractional free volume using the polymer density. A density value of 1.38 g/cm^3 was used in the present case [41], resulting in a predicted fractional free volume of 0.07. This value must be divided by the tortuosity to provide a value for the effective porosity. Given the tortuosity of a membrane is typically 1.5 to 2.5 [23] gives an estimate of between 0.03 and 0.05 for the effective porosity.

The model correctly predicts the increase in rejection of boron at higher pressures (Figure 9). At high applied pressures, the impact of convection is greater and the contribution of the bulk convection term becomes more apparent. This is evident from the modelling results shown in Figure 10.

In analysing the high pH region, where a portion of boric acid is ionised to borate ion, Equation 9 to Equation 16 are used to account for the contribution of electrochemical migration and Donnan potential (the calculation sequence is shown in Figure 3). The electrochemical potential difference across the membrane (Equation 10) is calculated by summing the contribution from both co-ions ($B(OH)_4^-$ and OH^-) and counter ions (H^+ and Na^+). The contribution of Na^+ and OH^- must be included as the concentration of NaOH is high relative to the concentration of boron in the feed solution (particularly at pH 11 and above). At these high pH values the OH^- binds H^+ and shifts Reaction 2 towards the right hand side, so that the dominant ions are OH^-, $B(OH)_4^-$ and Na^+. Experimental data with fitted results are shown in Figure 9 and Figure 11.

For $B(OH)_4^-$, the rejection is enhanced by the surface charge of the membrane so that the rejection approaches 100% (Figure 9). The increased rejection relative to the uncharged species is due to the additional contribution from the electro repulsion between the negatively charged membrane and $B(OH)_4^-$. Rejection is also increased by the large concentrations of OH^- present. This anion will permeate preferentially with the sodium cation, Na^+, due to its smaller size. It can also be seen that the effects of bulk convection are less important in this case, with rejection changing little in absolute terms as the pressure is increased.

At intermediate pH values (pH 8), the rejection of boron is modelled based upon the results for both the ionised species (pH 11) and the uncharged species (pH 3). That is, the total rejection is determined from (Figure 3):

$$[Rejection_{total} = Rejection_{boric\ acid} \times \%\ unionised\ boric\ acid|_{Steric} + Rejection_{borate\ ion} \times \%\ ionised\ boric\ acid\ |_{Donnan\ and\ Steric}]$$

At this pH, a small decrease in the rejection is observed experimentally when the boron concentration is increased from 1 to 20 mg/L (Figure 11). This is in contrast to the usual case where the rejection of solute increases with increasing feed concentration. In such cases, the water flux decreases due to the osmotic pressure difference, causing a relative increase in rejection. However, in the present work, the contribution of the osmotic pressure difference is negligible and the decrease can be attributed to changes in the relative percentages of charged and uncharged species.

That is, as the feed concentration increases, there is a percentage increase in the concentration of uncharged boric acid, which has a lower rejection.

4.4. The Effect of Total Salinity

When NaCl is present in the solution alongside boron, a decrease in rejection is observed (Figure 12) despite an increase in the total amount of charged borate ions (Figure 1). This trend was not clearly observed by Koseoglu et al [4]; however it was observed by Oo et al. [2] for a brackish water RO membrane. A decrease in the borate anion rejection is expected as charge repulsion of this ion is reduced by charge screening of the membrane surface. However, in the present case, the fall in rejection primarily reflects changes in the concentration of the neutral boric acid, as at pH 8.5 less than 20% of boron is ionised. Rejection of the neutral species falls due to the increase in osmotic pressure which reduces the permeate flux (J_v). This causes the permeate concentration to rise. The rejection of NaCl falls for identical reasons.

In modelling this system, the total potential difference (Equation 9) must also include contributions from the ions Na^+ and Cl^-. As depicted in Figure 4(b), the membrane streaming potential must also be adjusted for the increasing salinity, reaching a plateau at > 200 mM (> 11 g/L NaCl). This plateau is caused by the screening of the membrane charge by the accumulation of ions in the vicinity of the membrane surface. Measurement of zeta potential with electrolyte concentration lower than 1mM carries significant inaccuracy due to interference of surface conductance. On the contrary, beyond 100mM the voltage measurement is no longer sensitive causing greater than 4mV error reading. Therefore, in calculating the surface charge density beyond concentration of 100mM, the zeta potential is set to be constant. The results from this modelling are also shown in Figure 12. The fit is extremely good, given that no parameter optimisation has been undertaken. Some discrepancy at higher NaCl concentration is observed and this might be associated with inaccuracy in the measurement of streaming potential as stated above.

5. Conclusion

Experimental results for the permeation of boron through a reverse osmosis membrane have confirmed the findings of other authors, that such permeation requires the consideration of convective flow through a porous medium. In particular, the flux of boron increases with increasing water flux, a phenomenon that cannot be explained with a solution diffusion model. Analyses of boron rejection have been conducted by employing the model developed by Bowen and co-workers which utilises the Extended Nernst-Planck transport equation across the membrane. At low pH where boron primarily exists as neutral solute, the rejection is dictated by steric hindrance and found to be sensitive to the change in the pore size. The experimental data was satisfactorily fitted when a pore size of 0.380 nm was used with an effective membrane porosity of 0.05. At high pH where boric acid dissociates to form borate ions, the dependency on steric contribution and pressure is less evident. The surface charge results in high rejection of these ions (> 99%) at pH > 11. These effects can be modelled using experimental streaming potential data as the basis of the charge density in the membrane. The effect of salinity is also analysed utilising this model with no need for further fitting of any parameters.

This modelling calls into question the true mechanism for transport of solutes through a reverse osmosis membrane. The solution diffusion model has been successfully utilised for decades to describe both salt and water transport through such substrates. However, this model requires the pressure inside the membrane to be constant throughout, and for solutes to move independently of the solvent. This work has confirmed that boron does not move through the membrane independently of water – increasing the transmembrane pressure increases boron permeation through convective transfer with the water phase. Such convective flow requires a pressure difference across the membrane and so it is unclear how it can be rationalised with a solution diffusion approach.

6. Acknowledgements

The authors thank Lachlan Mason (PFPC, The University of Melbourne Australia) for his contribution in building the shell-frame for the MATLAB R 2009b code and Bio21 institute for TEM measurement. Financial support for this work was provided by the Australian Research Council Discovery Projects Scheme (DP1093815). The Particulate Fluids Processing Centre, a Special Research Centre of the Australian Research Council is also acknowledged for infrastructure support. AJH acknowledges the support of CSIRO's Office of the Chief Executive Science Leader program.

Nomenclature

Solute flux (membrane area basis)	j_s	**mg/ m² s**
Permeate flux (membrane area basis)	J_v	**m/s**
Bulk Diffusivity	D_∞	**m²/s**
Pore diffusivity component i	D_{ip}	**m²/s**
Hindrance factor of convention	K_{ic}	**-**
Hindrance factor of diffusion	K_{id}	**-**
Sorption Coefficient in the liquid phase	K^L	**-**
Bulk concentration of i	C_i	**mol/m³**
Pore concentration of i	c_i	**mol/m³**
Water permeability	**A**	**m/s Pa**
Solute permeability	**B**	**m/s**
Thickness of the membrane	x	**m**
Valence	z	**-**
Ionic Strength	**I**	**mol/m³**
Universal Gas Constant	**R**	**8.314 J/mol.K**
Absolute temperature	**T**	**K**
Faraday constant	**F**	**96487 C/mol**
Boltzman constant	k_b	**1.381×10^{-23} J/K**
Pore radius	r_p	**m**
Stokes radius	a_s	**m**
Hydrated ion radius	r_i	**m**
Electron Charge	**e**	**1.602192×10^{-19} C**
Dielectric constant of the electrolyte solution	ε_r	**-**
Avogadro's Constant	N_A	**6.022×10^{23} mol^{-1}**
Permittivity of vacuum	ϵ_0	**8.854185×10^{-12} C²/N.m²**
Dynamic viscosity of solution	η	**N s /m**
Ratio ion radius to pore radius	λ	**-**
Steric partitioning	ϕ	$(1-\lambda)^2$
Effective membrane charge density	X_d	**mol/m³**
Donnan potential	$\Delta\psi_D$	**V**
Electrokinetic surface charge density	σ_s	**C/m²**
Debye length	**1/k**	**m**
Staverman reflection coefficient	σ	**-**
Osmotic pressure	π	**Pa**
Solute partial molar volume	V_s	**m³ /mol**
Effective porosity	A_k	
	Subscript	
Component or ion i	i	
In the pore	p	
In the feed side	**f**	
In the permeate side	P	
Bulk condition	**b**	
On membrane surface (x= 0 or x = Δ l)	m	

References

[1] N. Kabay, S. Sarp, M. Yuksel, Ö. Arar, M. Bryjak, Removal of boron from seawater by selective ion exchange resins, Reactive and Functional Polymers, 67 (2007) 1643-1650.
[2] M.H. Oo, S.L. Ong, Implication of zeta potential at different salinities on boron removal by RO membranes, Journal of Membrane Science, 352 (2010) 1-6.
[3] P.P. Mane, P.-K. Park, H. Hyung, J.C. Brown, J.-H. Kim, Modeling boron rejection in pilot- and full-scale reverse osmosis desalination processes, Journal of Membrane Science, 338 (2009) 119-127.
[4] H. Koseoglu, N. Kabay, M. Yüksel, M. Kitis, The removal of boron from model solutions and seawater using reverse osmosis membranes, Desalination, 223 (2008) 126-133.
[5] O. Maung Htun, O. Say Leong, Boron removal and zeta potential of RO membranes: impact of pH and salinity, Desalination & Water Treatment, 39 (2012) 83-87.
[6] M. Rodríguez Pastor, A. Ferrándiz Ruiz, M.F. Chillón, D. Prats Rico, Influence of pH in the elimination of boron by means of reverse osmosis, Desalination, 140 (2001) 145-152.
[7] World Health Organisation, Boron in drinking water, Background document for development of WHO Guidelines for Drinking-water Quality, in, Geneva, 2003.
[8] L.J. Banasiak, A.I. Schäfer, Removal of boron, fluoride and nitrate by electrodialysis in the presence of organic matter, Journal of Membrane Science, 334 (2009) 101-109.
[9] Choi, Evaluation of boron removal by adsorption on solids, Environmental science & technology, 13 (1979) 189-196.
[10] M. Taniguchi, M. Kurihara, S. Kimura, Boron reduction performance of reverse osmosis seawater desalination process, Journal of Membrane Science, 183 (2001) 259-267.
[11] K.L. Tu, A.R. Chivas, L.D. Nghiem, Effects of membrane fouling and scaling on boron rejection by nanofiltration and reverse osmosis membranes, Desalination, 279 (2011) 269-277.
[12] K.L. Tu, L.D. Nghiem, A.R. Chivas, Boron removal by reverse osmosis membranes in seawater desalination applications, Separation and Purification Technology, 75 (2010) 87-101.
[13] K.L. Tu, L.D. Nghiem, A.R. Chivas, Coupling effects of feed solution pH and ionic strength on the rejection of boron by NF/RO membranes, Chemical Engineering Journal, 168 (2011) 700-706.
[14] O. Kedem, A. Katchalsky, A physical interpretation of the phenomenological coefficients of membrane permeability, The Journal Of General Physiology, 45 (1961) 143-179.
[15] H. Hyung, J.-H. Kim, A mechanistic study on boron rejection by sea water reverse osmosis membranes, Journal of Membrane Science, 286 (2006) 269-278.
[16] G.E. Jonsson, F. Macedonia, Fundamentals in reverse osmosis, in: E. Drioli (Ed.) Comprehensive Membrane Science and Engineering: Membrane operations in molecular separations, Elsevier Science (2010) 1-21.
[17] K.S. Spiegler, O. Kedem, Thermodynamics of hyperfiltration (reverse osmosis): criteria for efficient membranes, Desalination, 1 (1966) 311-326.
[18] E.M. Van Wagner, A.C. Sagle, M.M. Sharma, B.D. Freeman, Effect of crossflow testing conditions, including feed pH and continuous feed filtration, on commercial reverse osmosis membrane performance, Journal of Membrane Science, 345 (2009) 97-109.
[19] G. Jonsson, J. Benavente, Determination of some transport coefficients for the skin and porous layer of a composite membrane, Journal of Membrane Science, 69 (1992) 29-42.
[20] S. Kimura, Analysis of reverse osmosis membrane behaviors in a long-term verification test, Desalination, 100 (1995) 77-84.
[21] T. Hoang, G. Stevens, S. Kentish, The effect of feed pH on the performance of a reverse osmosis membrane, Desalination, 261 (2010) 99-103.
[22] J.G. Wijmans, R.W. Baker, The solution-diffusion model: a review, Journal of Membrane Science, 107 (1995) 1-21.
[23] R.W. Baker, Membrane technology and application, John Willey &Sons Ltd, Menlo Park, California, 2004.

[24] G.S. Rice, Membrane Separation of Calcium Salts from Dairy Ultrafiltration Process, in: Chemical and Biomolecular Engineering, The University of Melbourne, Melbourne, 2008.
[25] W.R. Bowen, A.W. Mohammad, N. Hilal, Characterisation of nanofiltration membranes for predictive purposes — use of salts, uncharged solutes and atomic force microscopy, Journal of Membrane Science, 126 (1997) 91-105.
[26] W.R. Bowen, J.S. Welfoot, Modelling the performance of membrane nanofiltration—critical assessment and model development, Chemical Engineering Science, 57 (2002) 1121-1137.
[27] W.R. Bowen, B. Cassey, P. Jones, D.L. Oatley, Modelling the performance of membrane nanofiltration—application to an industrially relevant separation, Journal of Membrane Science, 242 (2004) 211-220.
[28] S.L. Ong, W.W. Zhou, L.F. Song, W.J. Ng, Evaluation of feed concentration effects on salt/ion transport through RO/NF membranes with the Nernst-Planck-Donnan model, Environmental Engineering Science, 19 (2002) 429-439.
[29] S. Bouranene, P. Fievet, A. Szymczyk, M. El-Hadi Samar, A. Vidonne, Influence of operating conditions on the rejection of cobalt and lead ions in aqueous solutions by a nanofiltration polyamide membrane, Journal of Membrane Science, 325 (2008) 150-157.
[30] A.I. Cavaco Morão, A. Szymczyk, P. Fievet, A.M. Brites Alves, Modelling the separation by nanofiltration of a multi-ionic solution relevant to an industrial process, Journal of Membrane Science, 322 (2008) 320-330.
[31] H. Zhu, A. Szymczyk, B. Balannec, On the salt rejection properties of nanofiltration polyamide membranes formed by interfacial polymerization, Journal of Membrane Science, 379 (2011) 215-223.
[32] G. Hagmeyer, R. Gimbel, Modelling the rejection of nanofiltration membranes using zeta potential measurements, Separation and Purification Technology, 15 (1999) 19-30.
[33] M.J. Ariza, J. Benavente, Streaming potential along the surface of polysulfone membranes: a comparative study between two different experimental systems and determination of electrokinetic and adsorption parameters, Journal of Membrane Science, 190 (2002) 119-132.
[34] R.L. Bassett, A critical evaluation of the thermodynamic data for boron ions, ion pairs, complexes, and polyanions in aqueous solution at 298.15 K and 1 bar, Geochimica et Cosmochimica Acta, 44 (1980) 1151-1160.
[35] H. Corti, Properties of the borate ion in dilute aqueous solutionsJ Chem Soc Faraday I, J Chem Soc Faraday I, 76 (1980) 2179.
[36] N.N. Greenwood, B.S. Thomas, The chemistry of Boron, Pergamon, Oxford, England, 1973.
[37] L.M. Rowe, L.B. Tran, G. Atkinson, The effect of pressure on the dissociation of boric acid and sodium borate ion pairs at 25°C, Journal of Solution Chemistry, 18 (1989) 675-689.
[38] D. Dyrssen, I. Hansson, Ionic medium effects in sea water — A comparison of acidity constants of carbonic acid and boric acid in sodium chloride and synthetic sea water, Marine Chemistry, 1 (1973) 137-149.
[39] E. Kohei, S.N. Que, E.K. Sandra, W.S. Geoffrey, The effect of boric acid on the vapour liquid equilibrium of aqueous potassium carbonate, Fluid Phase Equilibria, 309 (2011) 109-113.
[40] W.R. Bowen, X. Cao, Electrokinetic effects in membrane pores and the determination of zeta-potential, Journal of Membrane Science, 140 (1998) 267-273.
[41] J. Lee, C.M.H. Doherti, A.J.Kentish, E.S., Water Vapor Sorption and Free Volume in the Aromatic Polyamide Layer of Reverse Osmosis Membranes Journal of Membrane Science, 425-426 (2013) 217-226.
[42] M.J. Ariza, J. Benavente, Rodrı, amp, x, E. guez-Castellón, L. Palacio, Effect of Hydration of Polyamide Membranes on the Surface Electrokinetic Parameters: Surface Characterization by X-Ray Photoelectronic Spectroscopy and Atomic Force Microscopy, Journal of Colloid and Interface Science, 247 (2002) 149-158.
[43] D.C. Grahame, The electrical double layer and the theory of electrocapillarity, Chemical Reviews, 41 (1947) 441-501.

[44] I. Sutzkover, D. Hasson, R. Semiat, Simple technique for measuring the concentration polarization level in a reverse osmosis system, Desalination, 131 (2000) 117-127.
[45] V. Freger, Swelling and Morphology of the Skin Layer of Polyamide Composite Membranes: An Atomic Force Microscopy Study, Environmental Science & Technology, 38 (2004) 3168-3175.
[46] V. Freger, Nanoscale heterogeneity of polyamide membranes formed by interfacial polymerization, Heterogenität im Nanobereich von Polyamid-Membranen, hergestellt durch Grenzflächenpolymerisation, 11 (2004) 4791.
[47] P.J. Scales, F. Grieser, T.W. Healy, L.R. White, D.Y.C. Chan, Electrokinetics of the silica-solution interface: a flat plate streaming potential study, Langmuir, 8 (1992) 965-974.
[48] D.J. Shaw, Introduction to Colloid and Surface Chemistry, Butterworth-Heinemann, Oxford, 1992.
[49] R.J. Hunter, Zeta potential in colloid science : principle and applications, Academic Press, London, 1981.
[50] D.C. Dow FilmTec, Reverse Osmosis membrane BW30LE-440 Specification Sheet, in: Form No. 609-00192-0408.
[51] M. Mänttäri, A. Pihlajamäki, M. Nyström, Effect of pH on hydrophilicity and charge and their effect on the filtration efficiency of NF membranes at different pH, Journal of Membrane Science, 280 (2006) 311-320.
[52] M. Dalwani, N.E. Benes, G. Bargeman, D. Stamatialis, M. Wessling, Effect of pH on the performance of polyamide/polyacrylonitrile based thin film composite membranes, Journal of Membrane Science, 372 (2011) 228-238.
[53] Childress, Relating Nanofiltration Membrane Performance to Membrane Charge (Electrokinetic) Characteristics, Environmental science & technology, 34 (2000) 3710-3716.
[54] A. María Fernanda Chillón, B. Laureano Valero i, R. Daniel Prats, G. Pedro Varó, Kinetic behaviour of sodium and boron in brackish water membranes, Journal of Membrane Science, 368 (2011) 86-94.
[55] W. Richard Bowen, A. Wahab Mohammad, A theoretical basis for specifying nanofiltration membranes — Dye/salt/water streams, Desalination, 117 (1998) 257-264.
[56] A.A. Bondi, Physical properties of molecular crystals, liquids, and glasses, Wiley, New York, 1968.
[57] S. Bandini, D. Vezzani, Nanofiltration modeling: the role of dielectric exclusion in membrane characterization, Chemical Engineering Science, 58 (2006) 3303-3326.
[58] D. David, H. Ingemar, Research paper: Ionic medium effects in sea water — A comparison of acidity constants of carbonic acid and boric acid in sodium chloride and synthetic sea water, Marine Chemistry, 1 (1973) 137-149.
[59] E.R. Nightingale, Phenomenological theory of ion-solvation. Effective radii of hydrated ions, The Journal of Chemical Physics, 63 (1959) 1381-1387.
[60] E.L. Cussler, Diffusion : mass transfer in fluid systems / E.L. Cussler, Cambridge : Cambridge University Press, 2009. 3rd ed., 2009.
[61] K. Das, Single ionic partial molar volumes and solvation of ions, Journal of Solution Chemistry, 18 (1989) 1085-1093.
[62] G. Jákli, Evaluation of individual ionic partial molar volumes in aqueous solutions, The Journal of Chemical Thermodynamics, 40 (2008) 770-776.
[63] Y. Marcus, Volumes of Aqueous Hydrogen and Hydroxide Ions at 0 to 200 Â°C, The Journal of Chemical Physics, 137 (2012) 154501.
[64] M. Taniguchi, M. Kurihara, S. Kimura, Behavior of a reverse osmosis plant adopting a brine conversion two-stage process and its computer simulation, Journal of Membrane Science, 183 (2001) 249-257.

Table Captions

Table 1. The convective hindrance factor(K_{ic}) and diffusive hindrance factor (D_{ic}), based on the ratio of solute to pore radius (λ) [57].

Table **2**. Data used in modelling. For consistency, Stokes radii were utilised [26]. Boric acid was modelled with a radius of 2.61 Å which is equivalent to the radius of the borate ion. This is due to the data for boric acid being unavailable. Furthermore, it is claimed that the hydrated size of boric acid and borate ion are comparable as the boric acid is poorly hydrated due to its large crystal radius [12].

Figure Captions

Figure 1. Degree of dissociation of boric acid with respect to pH and salinity. The pKa for boric acid as a function of salinity is obtained from Dyrssen and Hansson 1972 [58].

Figure 2. Schematic diagram of the cross flow filtration rig.

Figure 3. Sequence of calculation. Pore radius and effective porosity have been previously determined by averaging over 50 data points using neutral solute rejection and flux data (from pH 2-4) and using Equation 4 and Equation 8.

Figure 4. Zeta potential data (a) as a function of pH at a background electrolyte concentration ≈ 0.6 g/L (10mM) NaCl and (b) as a function of NaCl concentration at pH 8.5.

Figure 5. Charge density (C/m^2): (a) as a function of pH at a constant ionic strength ≈ 0.6 g/L (10mM) NaCl and (b) at pH ≈ 8.5 as a function of NaCl concentration.

Figure 6. Water flux at constant pH≈ 8.5.

Figure 7. Rejection of boron as a function of pH at constant applied P of 1200 kPa, constant boron feed concentration of 4mg/L and no NaCl. The symbols represent experimental data, while the curves indicate simulations with different pore radii (r_p). Membrane thickness : 105nm

Figure 8. Solute flux versus applied pressure at pH 2.0 and 8.3, showing that the solute permeation increases linearly with increasing water flux and thus that the solution diffusion model is no longer valid.

Figure 9. Rejection of borate ion (pH ≈ 11.0) and boric acid (pH ≈ 2.0). Symbols are experimental data while the lines represent model simulations. Optimised pore radius is 0.380 nm (averaged over 50 data points) and experimental surface charge values are from Figure 4.

Figure 10. The proportion of the total flux of uncharged boric acid that can be attributed to both convection and diffusion as a function of water flux, based on model simulations. Convection has a more dominant effect at higher applied pressures, reflecting the greater water flows through the membrane. Membrane thickness : 105nm, r_p : 0.380nm.

Figure 11. Rejection of boron as a function of boron concentration for different applied pressures. In all the experiments, the pH ≈ 8.1 and the salinity is zero. Symbols represent experimental data, while

the lines represent model simulations. In modelling, a pore radius of 0.380nm and thickness of 105 nm is used.

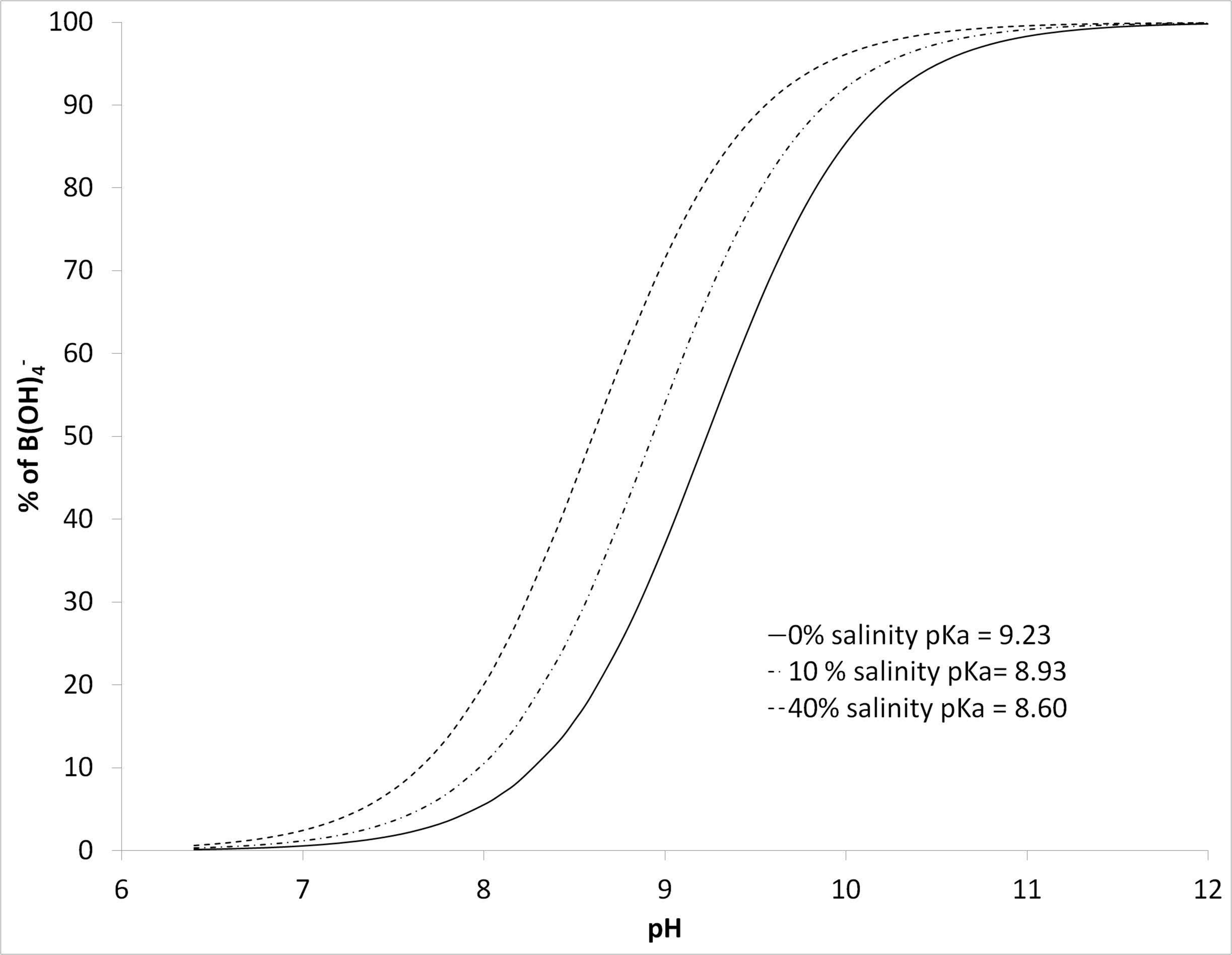
Figure 12. Rejection of NaCl and Boron, with constant P = 1200 kPa and pH ≈ 8.5, Boron concentration in feed ≈ 4 mg/L. Dotted lines represent values obtained from the mathematical model with r_p = 0.380nm.

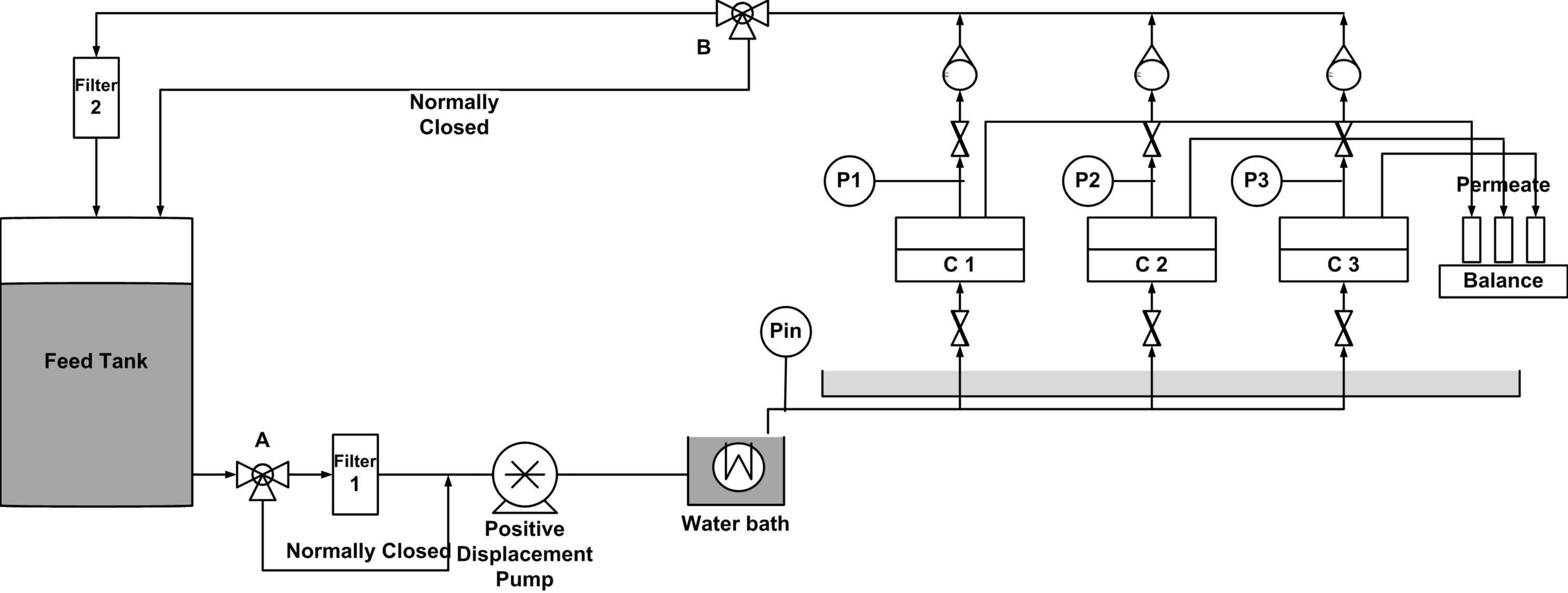
Table 1. The convective hindrance factor(Kic) and diffusive hindrance factor (Dic), based on the ratio of solute to pore radius ($\lambda_)$ [57].

$0 < (\lambda_i = r_i/r_p) \leq 0.8$	$0.8 < (\lambda_i = r_i/r_p) \leq 1$
$K_{ic} = -1.0 + 0.054\,\lambda_i - 0.988\,\lambda_i^2 + 0.441\,\lambda_i^3$ $K_{id} = 1.0 - 2.30\,\lambda_i + 1.154\,\lambda_i^2 + 0.224\,\lambda_i^3$	$K_{ic} = -6.83 + 19.348\,\lambda_i - 12.518\,\lambda_i^2$ $K_{id} = -0.105 + 0.318\,\lambda_i - 0.213\,\lambda_i^2$

Table 2. Data used in modelling. For consistency, Stokes radii were utilised [26]. Boric acid was modelled with a radius of 2.61 Å which is equivalent to the radius of the borate ion. This is due to the data for boric acid being unavailable. Furthermore, it is claimed that the hydrated size of boric acid and borate ion are comparable as the boric acid is poorly hydrated due to its large crystal radius [12].

	Stokes radius (Å)	Partial Molar Volume (V_{is}) cm^3/mol	Diffusion coefficient x 10^{-9} m^2/s	Reference
Na^+	1.84	-1.2	1.34	[26, 59, 60]
Cl^-	1.21	17.8	2.03	[26, 59, 60]
H^+	0.28	-5.4	9.33	[59-63]
OH^-	0.46	1.2	5.27	[59-63]
$B(OH)_4^-$	2.61	29.2	1.62	[8, 12, 35, 64]
H_3BO_3	-	39.2	1.47	[8, 12, 35, 64]
H_2O	1.4		-	[26, 61]
Membrane	3.80 (100%			This work


100
90
80
70
60
50
40
30
20
10
0
% of B(OH)4-
6
7
8
9
10
11
12
pH
—0% salinity pKa = 9.23
10 % salinity pKa= 8.93
--40% salinity pKa = 8.60


Filter
2
B
Normally
Closed
P1
P2
P3
Permeate
C 1
C 2
C 3
Balance
Pin
Feed Tank
A
Filter
1
Positive
Displacement
Pump
Water bath
Normally Closed

Input parameters:

Preliminary data : J_v (experimental water permeability), pH, T, P
Solute : $D_{ip,}$ K_{ic}, K_{id}, r_{stokes}, $C_{f\ B(OH)4-}$, $C_{f\ H3BO3}$
Membrane : ζ , r_{pore} , thickness Δx

Determine portion of dissociated boric acid based on pKa boric acid at given salinity. Portrayed in Figure 1.

Borate ion

Calculate X_d using zeta-potential data and Equation 13-15

Guess C_{ip}

Solve $\Delta\psi_{D\ at\ x\ =\ 0}$ and $\Delta\psi_{D\ at\ x\ =\Delta l}$ from partition coefficient equations (16) by assuming electroneutrality within the membrane (Equation 12)

Integrate Equation 9 to obtain calculated $c_{i\ at\ x\ =\ \Delta\ l}$

Calculate C_{ip} using calculated $\Delta\psi_{D\ at\ x\ =\Delta l}$

Compare guessed and calculated C_{ip} and minimize sum of square error

$SSE > 10^{-18}$

$SSE \leq 10^{-18}$

Calculate $R_{prediction\ of\ ion}$ =
$(1- C_{ip\ predicted} / C_{f\ input\ ion}) \times 100\%$

Compare $R_{theoretical}$ and $R_{experimental}$

Boric acid

Guess C_{ip}

Calculate steric partition coefficient and $c_{i\ at\ x\ =\ 0}$ (Equation 16)

Integrate Equation 9 to obtain calculated $c_{i\ at\ x\ =\ \Delta\ l}$

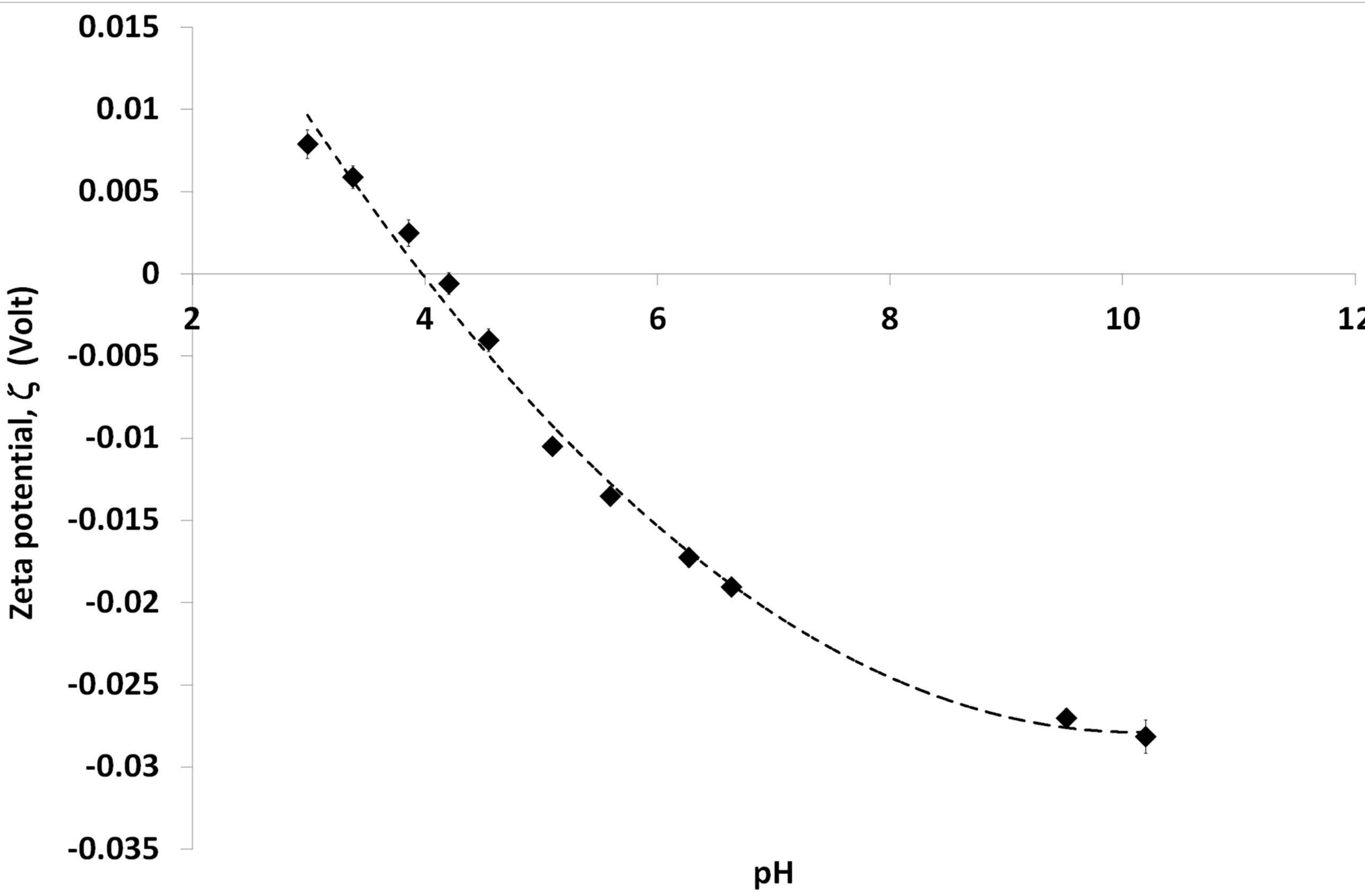
Compare guessed and calculated C_{ip} and minimize sum of square error

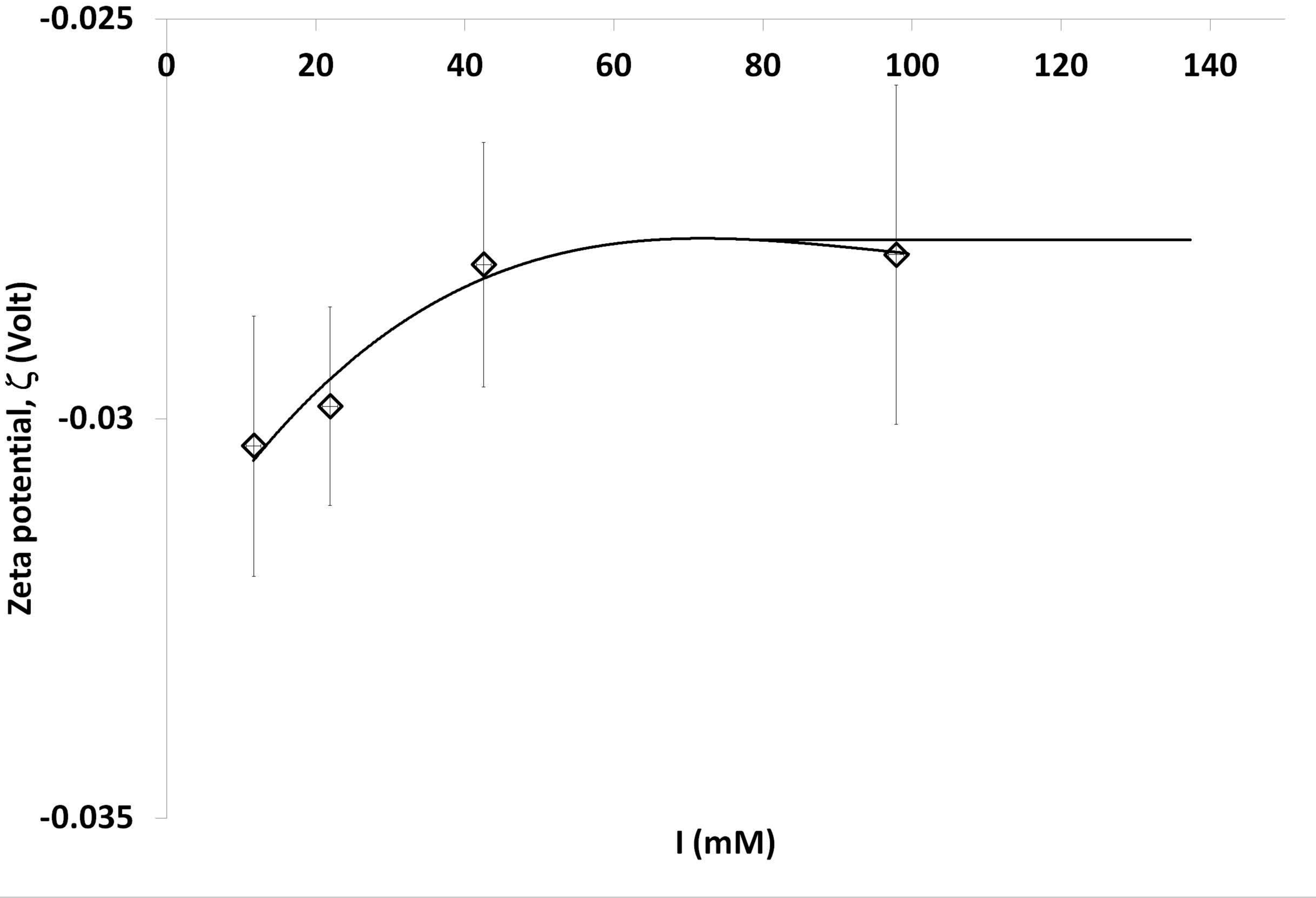
$SSE > 10^{-18}$

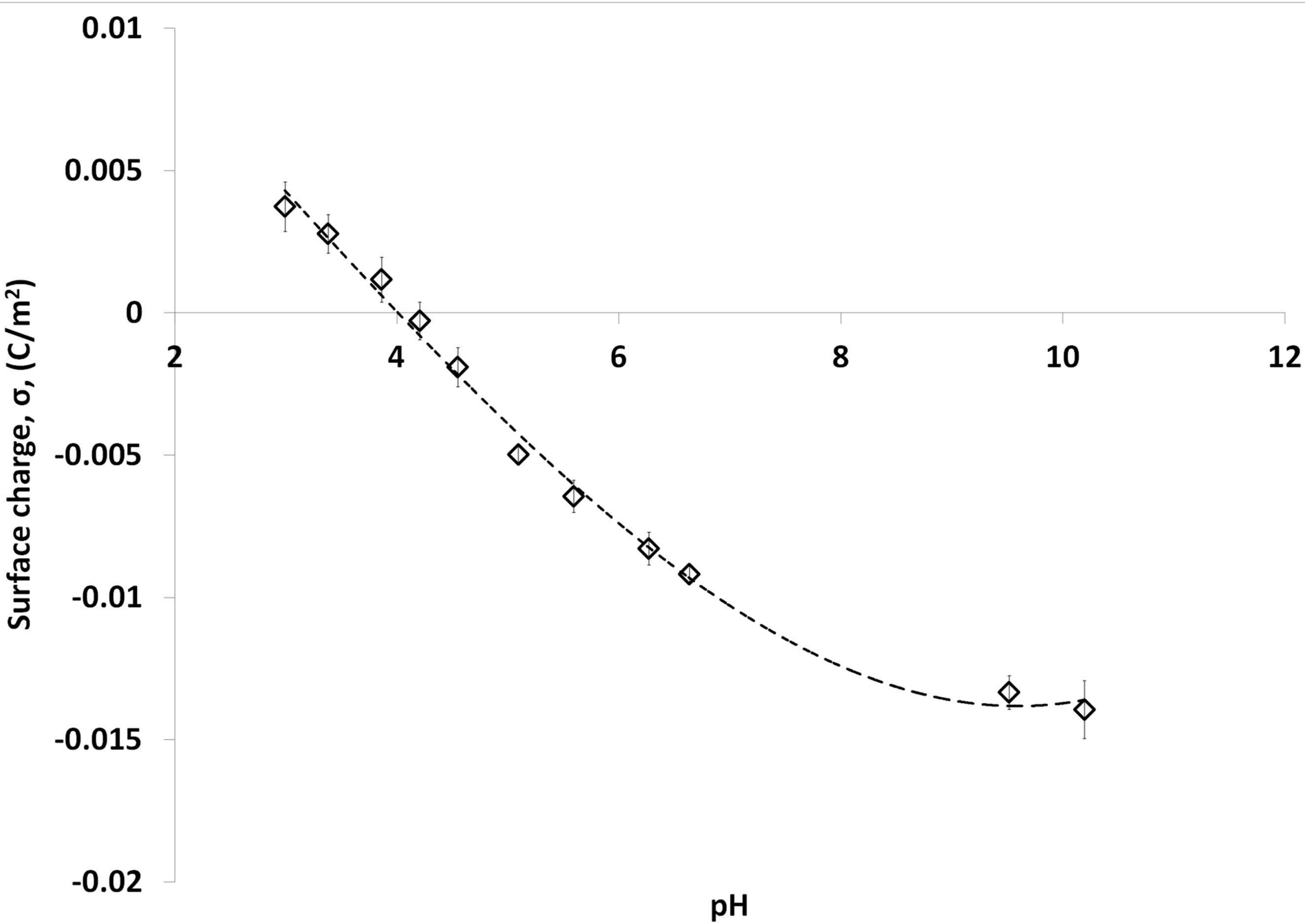
$SSE \leq 10^{-18}$

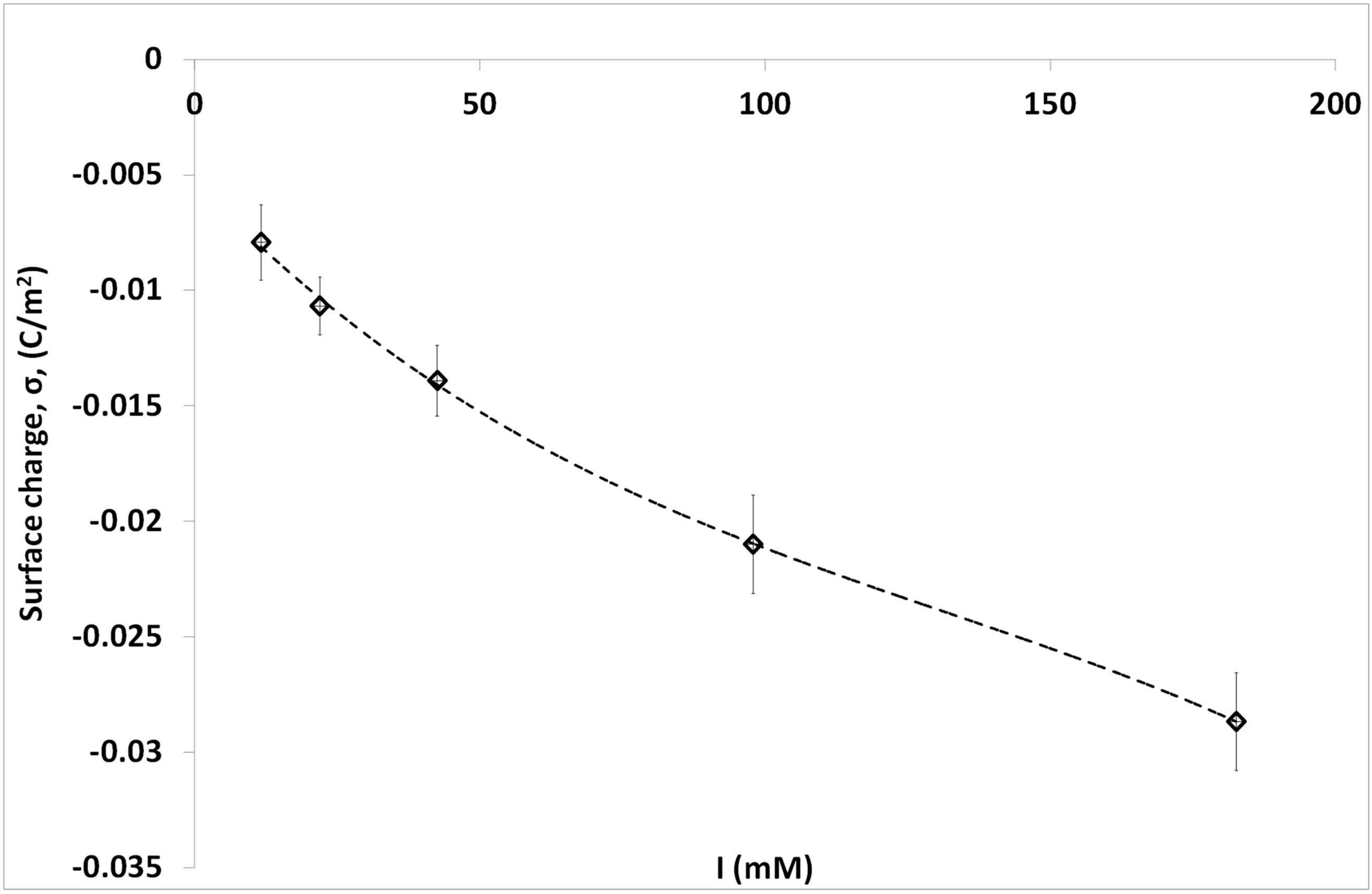
Calculate $R_{prediction\ of\ ion}$ =
$(1- C_{ip\ predicted} / C_{f\ input\ neutral\ solute}) \times 100\%$

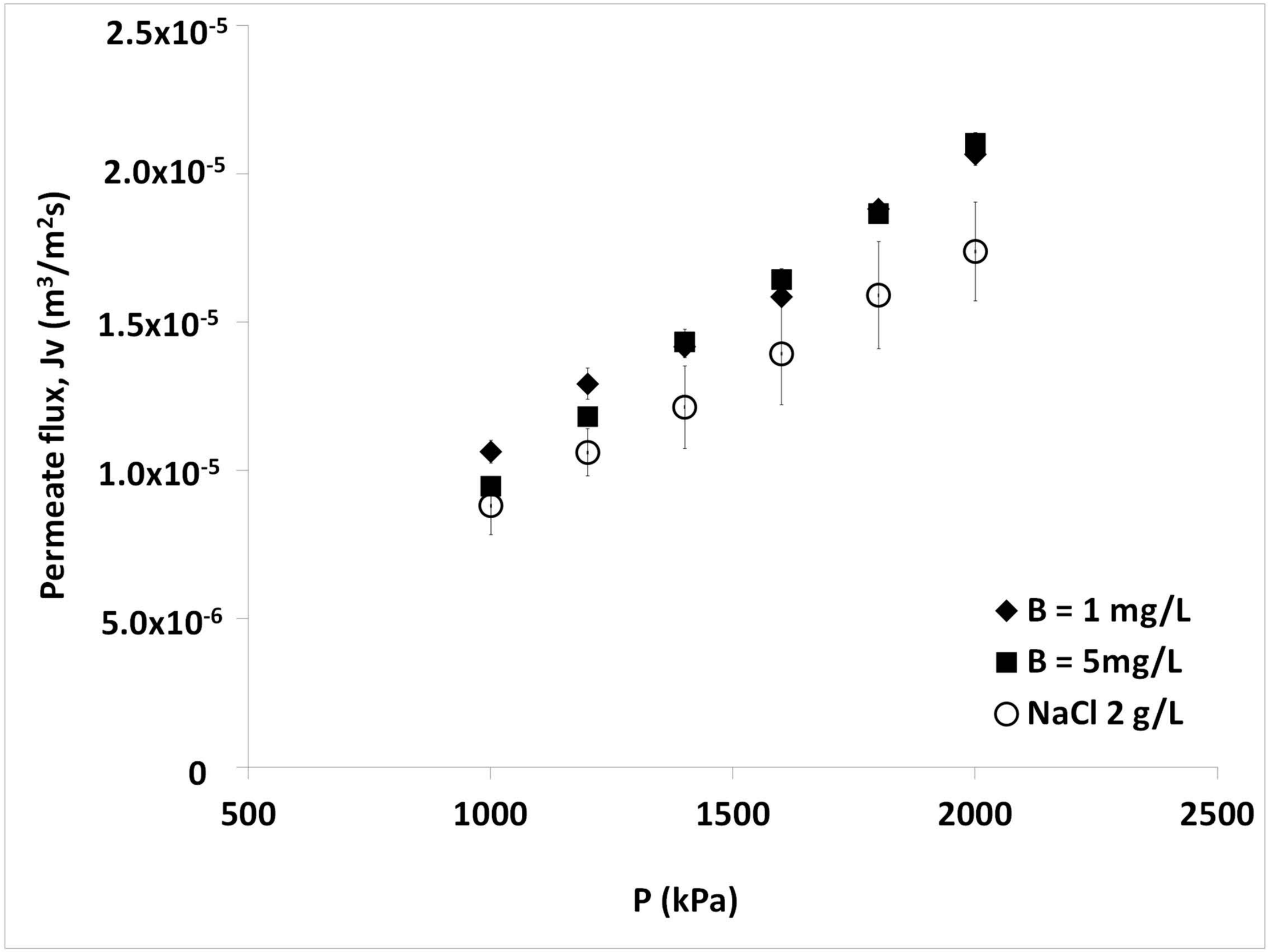
Compare $R_{theoretical}$ and $R_{experimental}$
If $R_{\ theoretical} \neq R_{experimental}$ = Modified r_{pore}

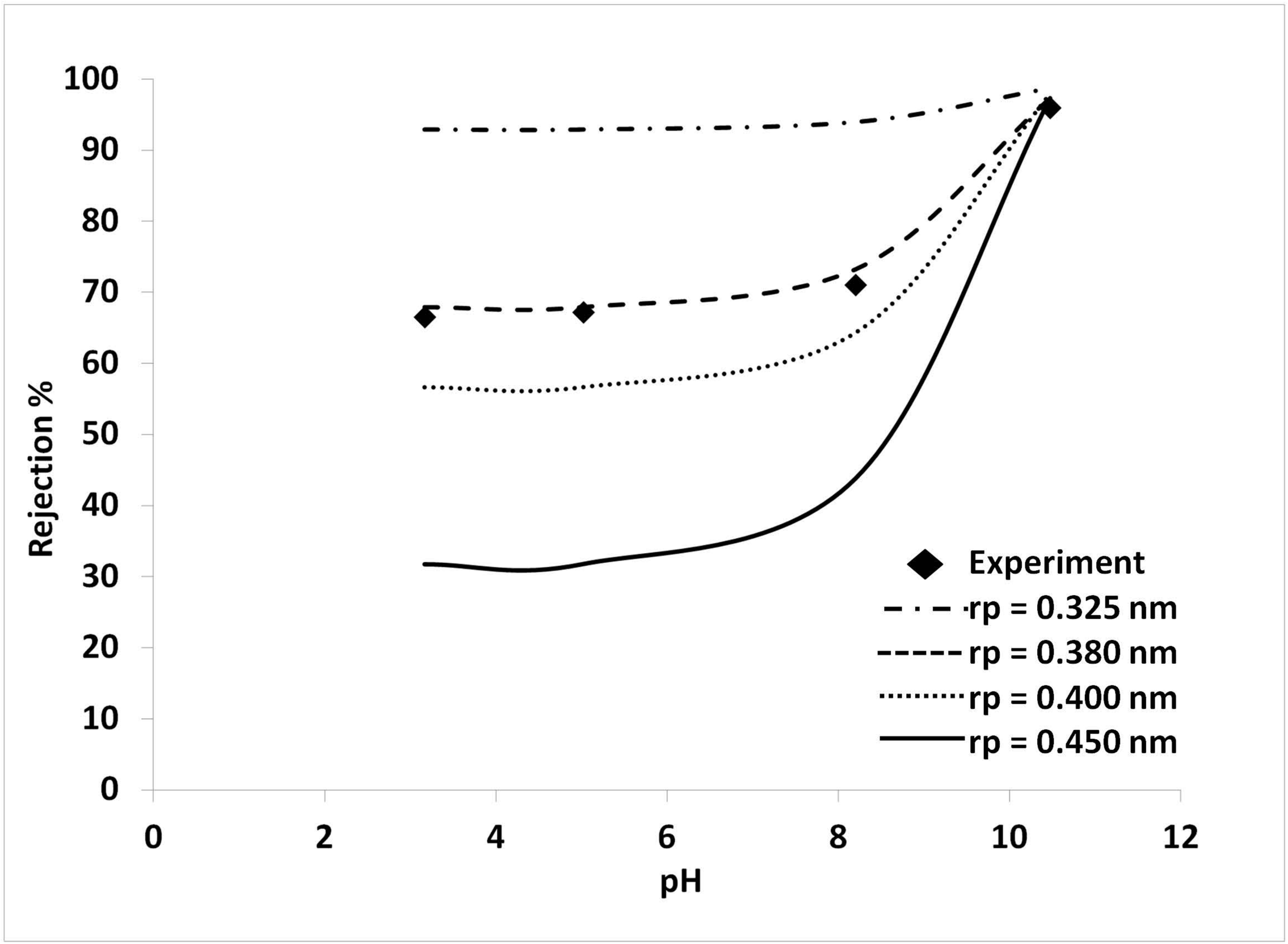

0.015
0.01
0.005
0
-0.005
-0.01
-0.015
-0.02
-0.025
-0.03
-0.035
2
4
6
8
10
12
Zeta potential, ζ (Volt)
pH

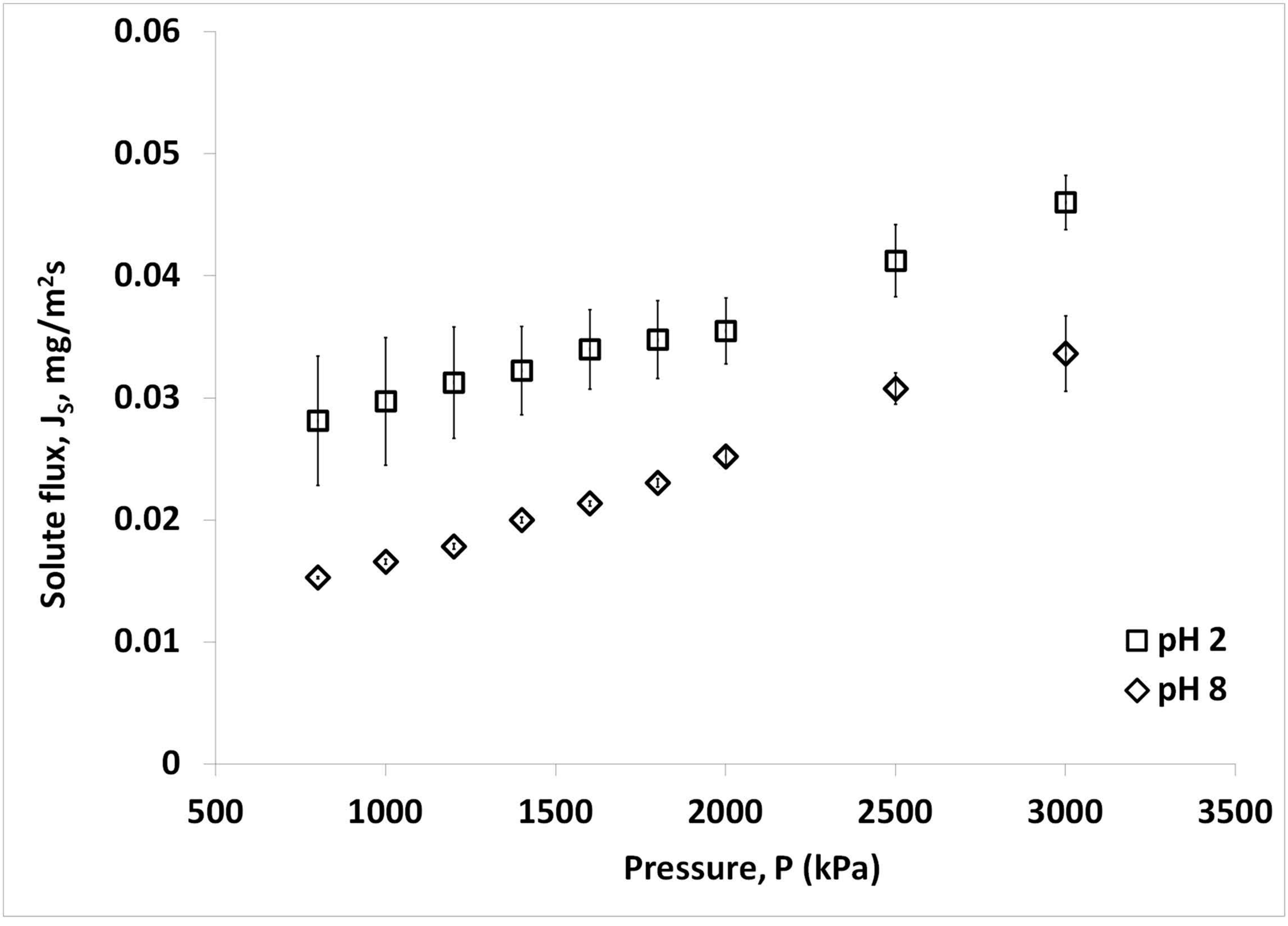

-0.025
0
20
40
60
80
100
120
140
Zeta potential, ζ (Volt)
-0.03
-0.035
I (mM)

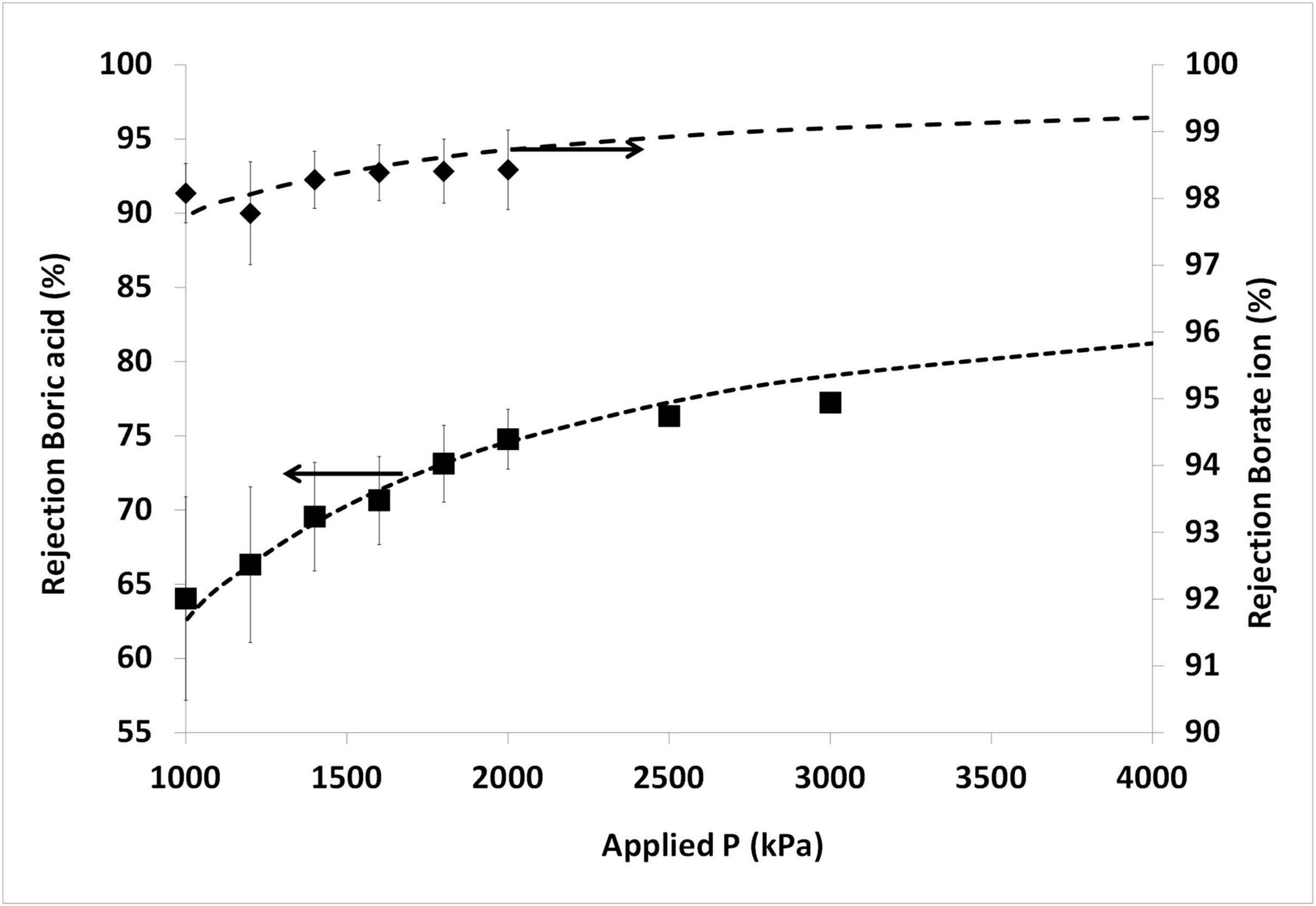

0.01
0.005
0
-0.005
-0.01
-0.015
-0.02
2
4
6
8
10
12
Surface charge, σ, (C/m²)
pH

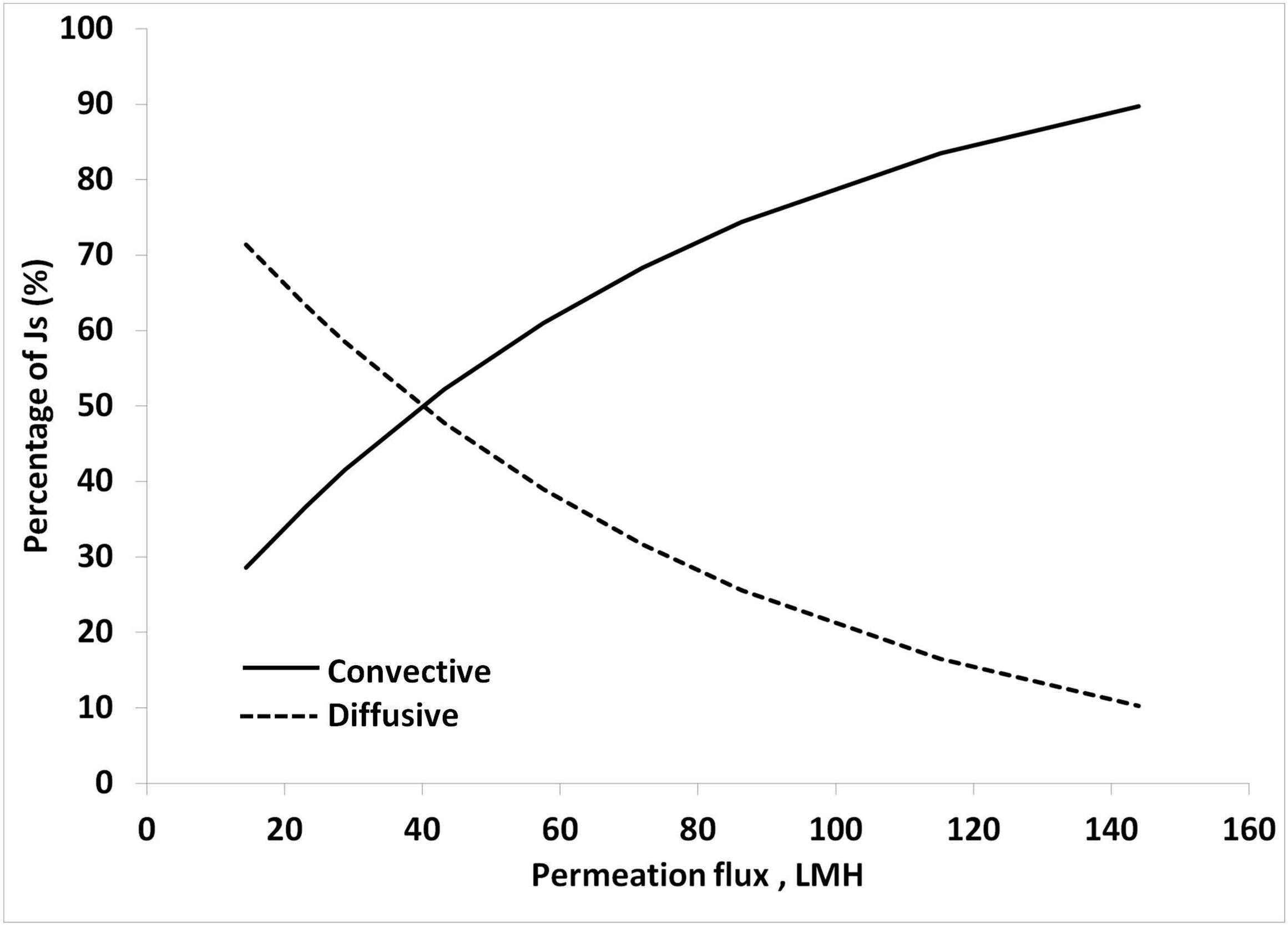

0
0
50
100
150
200
-0.005
-0.01
-0.015
-0.02
-0.025
-0.03
-0.035
Surface charge, σ, (C/m²)
I (mM)

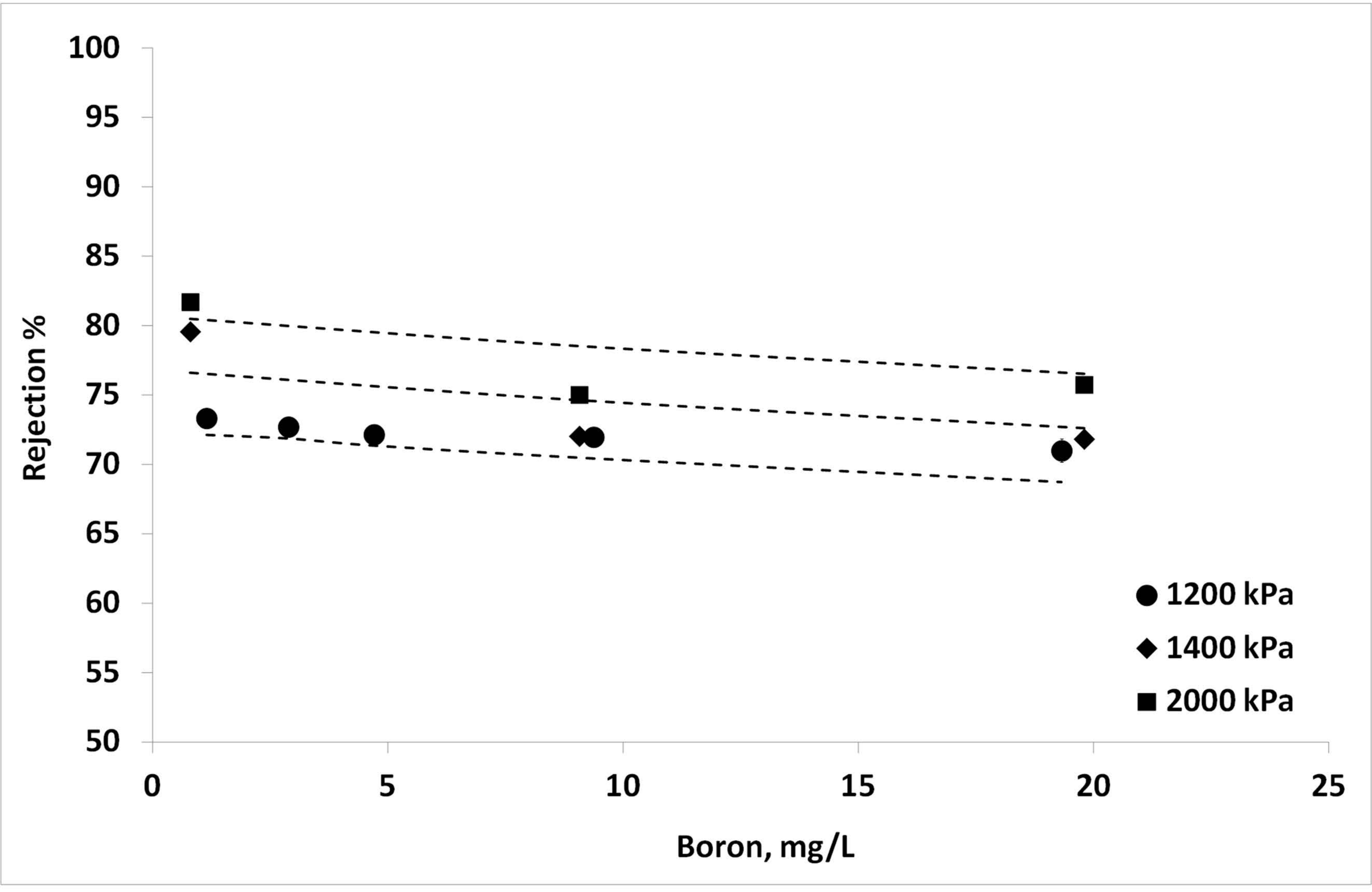

2.5x10-5
2.0x10-5
1.5x10-5
1.0x10-5
5.0x10-6
0
Permeate flux, Jv (m3/m2s)
500
1000
1500
2000
2500
P (kPa)
B = 1 mg/L
B = 5mg/L
NaCl 2 g/L

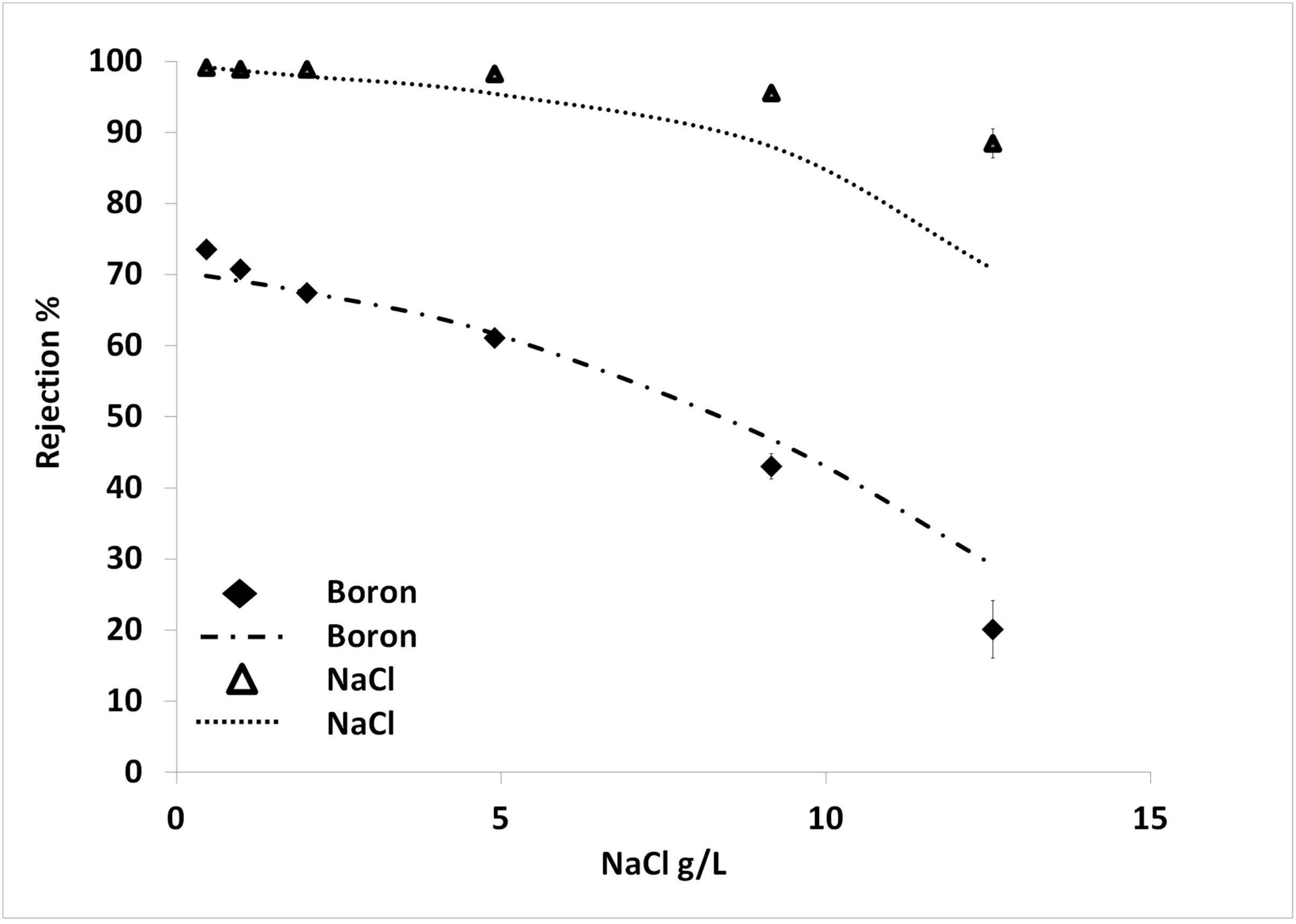

100
90
80
70
60
50
40
30
20
10
0
Rejection %
0
2
4
6
8
10
12
pH
Experiment
rp = 0.325 nm
rp = 0.380 nm
rp = 0.400 nm
rp = 0.450 nm


0.06
0.05
0.04
0.03
0.02
0.01
0
Solute flux, J_s, mg/m^{2}s
500
1000
1500
2000
2500
3000
3500
Pressure, P (kPa)
pH 2
pH 8


100
95
90
85
80
75
70
65
60
55
Rejection Boric acid (%)
100
99
98
97
96
95
94
93
92
91
90
Rejection Borate ion (%)
1000
1500
2000
2500
3000
3500
4000
Applied P (kPa)


100
90
80
70
60
50
40
30
20
10
0
Percentage of Js (%)
0
20
40
60
80
100
120
140
160
Permeation flux , LMH
Convective
Diffusive


100
95
90
85
80
75
70
65
60
55
50
Rejection %
0
5
10
15
20
25
Boron, mg/L
1200 kPa
1400 kPa
2000 kPa


100
90
80
70
60
50
40
30
20
10
0
Rejection %
0
5
10
15
NaCl g/L
Boron
Boron
NaCl
NaCl